Moisture Source Changes Contributed to Different Precipitation Changes over the Northern and Southern Tibetan Plateau

CHI ZHANG,[a,b] QIUHONG TANG,[a,c] DELIANG CHEN,[d,e] RUUD J. VAN DER ENT,[f,g] XINGCAI LIU,[a] WENHONG LI,[h] AND GEBREMEDHIN GEBREMESKEL HAILE[a]

[a] *Key Laboratory of Water Cycle and Related Land Surface Processes, Institute of Geographic Sciences and Natural Resources Research, Chinese Academy of Sciences, Beijing, China*
[b] *Key Laboratory of Land Surface Pattern and Simulation, Institute of Geographic Sciences and Natural Resources Research, Chinese Academy of Sciences, Beijing, China*
[c] *University of Chinese Academy of Sciences, Beijing, China*
[d] *Regional Climate Group, Department of Earth Sciences, University of Gothenburg, Gothenburg, Sweden*
[e] *CAS Center for Excellence in Tibetan Plateau Earth Sciences, Chinese Academy of Sciences, Beijing, China*
[f] *Department of Water Management, Faculty of Civil Engineering and Geosciences, Delft University of Technology, Delft, Netherlands*
[g] *Department of Physical Geography, Faculty of Geosciences, Utrecht University, Utrecht, Netherlands*
[h] *Earth and Ocean Sciences, Nicholas School of the Environment, Duke University, Durham, North Carolina*

(Manuscript received 8 May 2018, in final form 13 December 2018)

ABSTRACT

Precipitation on the Tibetan Plateau (TP) showed different spatial changes during 1979–2016, with an increasing trend over the northern Tibetan Plateau (NTP) and a slightly negative trend over the southern Tibetan Plateau (STP). The changes in precipitation moisture sources over the NTP and STP are investigated using the improved Water Accounting Model with an atmospheric reanalysis as well as observational precipitation and evaporation data. The results show the region in the northwest (region NW), ranging from the TP to Europe dominated by the westerlies, provides 38.9% of precipitation moisture for the NTP, and the region in the southeast (region SE), ranging from the TP to the Indian Ocean and Indochina dominated by the Asian monsoons, provides 51.4% of precipitation moisture for the STP. For the precipitation increase over the NTP, the SE and TP are the main contributors, contributing around 35.8% and 51.7% of the increase, respectively. The contributions from the SE and TP to the STP are, however, minor and insignificant. Meanwhile, the NW shows a negative trend of $-4.2 \pm 2.9\,\mathrm{mm\,yr^{-1}\,decade^{-1}}$ (significant at the 0.01 level), which contributes to the negative precipitation trend over the STP. Results during the wet season indicate that moisture sources from the areas dominated by the Asian monsoons have contributed more precipitated moisture for the NTP, but not for the STP. Further analysis reveals that precipitated moisture originating from the Indian subcontinent has increased for the NTP while it has decreased for the STP during 1979–2016.

1. Introduction

The Tibetan Plateau (TP), as the ''Third Pole,'' plays an important role in regional and hemispheric climate (Xu et al. 2014). Its environmental changes also draw the worldwide interests in the academic society (Boos and Kuang 2010; Yao et al. 2012; Sun and Ding 2011; Cuo et al. 2013; Klein et al. 2014; Bibi et al. 2018). Recently, it has been established that, although there has been an overall wetting over the TP under global warming (Chen et al. 2015; Zhang et al. 2017a; Yang et al. 2011), changes in precipitation appear to be regional (Krause et al. 2010; Yin et al. 2012; Gao et al. 2014). Liu and Yin (2001) observed an antiphase of summer precipitation variations between the northeast and southeast of the Tanggula Mountains. Chen et al. (2015) pointed out a marked precipitation difference between the northern and southern TP (NTP and STP) as precipitation is increasing over the NTP while decreasing in the STP. Feng and Zhou (2012) also found a dipole pattern in summer precipitation changes between the NTP and STP. More studies suggest a general wetting trend over the northwestern TP and a drying trend over

Supplemental information related to this paper is available at the Journals Online website: https://doi.org/10.1175/JHM-D-18-0094.s1.

Corresponding author: Qiuhong Tang, tangqh@igsnrr.ac.cn

DOI: 10.1175/JHM-D-18-0094.1

the southeastern TP (Cuo et al. 2013; Yin et al. 2012; Gao et al. 2015).

As the climatological precipitation generally decreases from the humid southeast to the arid northwest (Yang et al. 2011; Gao et al. 2015), the argument "wet gets wetter and dry gets drier" seems not valid in the TP (Held and Soden 2006; Seager and Vecchi 2010). Moreover, as Yao et al. (2013) pointed out, the NTP is mainly influenced by the westerlies, while the STP is controlled by the monsoons. Different circulations bring in different sources of moisture to the TP. The moisture sources for precipitation in the TP have been studied in the past. Chen et al. (2012) identified the primary moisture sources of precipitation over the TP, which include regions from the Indian subcontinent to the Southern Hemisphere, the Bay of Bengal, and the northwestern part of the TP. However, contributions from different source regions were not quantified. Sun and Wang (2014) quantified the moisture contributions from different sources to the eastern TP precipitation by using the areal source-receptor attribution method. The results indicate that moisture released over the eastern TP mostly comes from the Eurasian continent. Although moisture uptake from oceanic sources is considerable, much is lost en route. Similar conclusions are drawn for precipitation over the central-western TP (Zhang et al. 2017a). However, the recent precipitation increase in the central-western TP is mainly attributed to the strengthened moisture transport from the Indian Ocean and the intensified local moisture recycling (Zhang et al. 2017a). The intensified local recycling in the central-western TP is also validated by isotope data, as An et al. (2017) found a significant increase in local recycling during the past decades in the two ice core sites within this area.

Despite the progress made so far, sources and the quantified contributions for precipitation over the STP remain unknown, not to mention the difference between the NTP and STP. Further, the differences in precipitation trends over the STP and NTP might indicate different changes in both circulations and moisture sources which have not been systematically studied before. In view of these, this study focuses on the moisture sources and their change with circulations for both NTP and STP. We first quantify the volumes of moisture from sources contributing to the precipitations of NTP and STP, and then analyze the trends of moisture contribution to reveal the mechanism that forms different precipitation variations.

2. Data, model, and methods

a. Data and study area

A ground-based 0.5° gridded monthly precipitation dataset from the China Meteorological Administration (CMA) is used (Zhao et al. 2014; Zhao and Zhu 2015). This dataset is derived from quality-controlled station records from ~2400 stations over China since 1961, out of which data from 1979 to 2016 are used. The grid interpolation has used the thin-plate smooth spline method by considering the elevation effects. The 3-hourly, 1° gridded evaporation fields from the Community Land Model in the Global Land Data Assimilation Systems (GLDAS; Rodell et al. 2004) dataset are chosen as GLDAS outperforms other reanalyses on surface variables (Wang and Zeng 2012; Gao et al. 2014). Because of the strong and suspicious anomaly in GLDAS in 1996 that is caused by the erroneous precipitation data (Zhou et al. 2013), the evaporation fields in 1996 are excluded from the analysis. The European Centre for Medium-Range Weather Forecasts (ECMWF) interim reanalysis (ERA-I; Dee et al. 2011) of $1° \times 1°$ spatial resolution is selected as it has a better performance among the reanalyses in simulating the atmospheric water budget over the TP (Gao et al. 2014) and other regions (Trenberth et al. 2011; Rienecker et al. 2011; Lorenz and Kunstmann 2012). ERA-I provides a suite of data, including the 6-hourly model-level zonal winds, meridional winds, and specific humidity; 6-hourly surface pressure and a set of vertically integrated moisture and flux variables (vertically integrated water, vertically integrated northward/eastward water fluxes in forms of vapor, liquid, and ice); and 3-hourly precipitation and evaporation.

Based on isotope observations over the TP, Yao et al. (2013) divided the TP into three climate zones by the latitudes, which are the westerlies domain (i.e., the NTP, north of 35°N), the monsoon domain (the STP, south of 30°N), and the transition domain in between. This study follows Yao et al.'s division to trace and compare the respective moisture sources for precipitation in the NTP and STP. These locations are shown in Fig. 1a. The topographic height data are provided by the Global Land One-km Base Elevation Project (https://www.ngdc.noaa.gov/mgg/topo/globe.html). According to CMA, the stations in NTP are mainly distributed in the east, while they are sparse in the west with only one station near the west boundary. For the STP, the stations are more evenly distributed. Thus, precipitation is likely to be more accurate in the STP than in the NTP.

b. WAM-2layers and experiment design

1) WAM-2LAYERS

Water Accounting Model-2layers (WAM-2layers) is an Eulerian model on moisture recycling, which can track moisture either forward or backward in time to

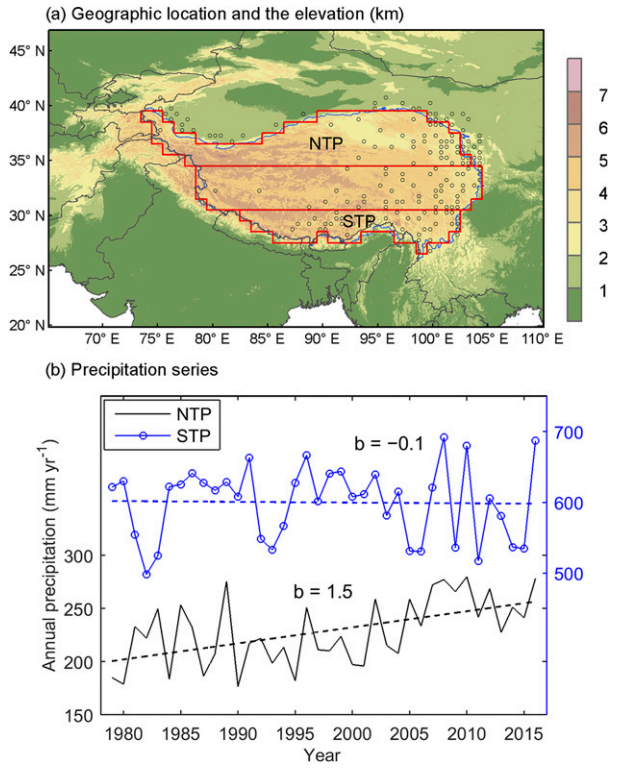

FIG. 1. (a) Geographic location of the STP and NTP, and the TP (blue line; the outer red box is the 1° × 1° discretion of the blue curve). The circles indicate the locations of stations in the CMA dataset on and near the TP. (b) The areal precipitation series of the STP and NTP from 1979 to 2016. The dashed lines represent the linear trends of the annual precipitation over the years, and *b* represents the slope of the best fit line.

quantify the moisture source–sink relations (van der Ent et al. 2013, 2014; van der Ent and Tuinenburg 2017). It is different from Lagrangian models that track moisture on the particle trajectories (Stohl and James 2004, 2005; Sodemann et al. 2008; Draxler and Hess 1998; Wei et al. 2012; Dirmeyer et al. 2014). WAM-2layers is an updated version of the original WAM. WAM is a 2D configuration that applies the ''well mixed'' assumption to the vertically integrated moisture and fluxes (van der Ent et al. 2010, 2013; Goessling and Reick 2013). In fact, the well-mixed conditions of moisture in the atmospheric column are usually not met (Bosilovich 2002; Goessling and Reick 2013). When there is strong wind shear in the vertical, substantial errors may occur (Goessling and Reick 2013; van der Ent et al. 2013). By dividing the vertical layer into two layers (i.e., WAM-2layers), van der Ent et al. (2013) showed an accurate reproduction of moisture tracking from a detailed 3D model (Knoche and Kunstmann 2013) in an area with high wind shear. Hence, moisture backtracking of WAM-2layers is applied in this study to track the moisture sources of the NTP and STP precipitations. The basic algorithm for backtracking is described briefly as follows.

Precipitation enters and evaporation exits the atmospheric water buckets. The fallen precipitation in the target area returns to the lower and upper buckets of air as ''tagged water'' in the model. The tagged water is mixed into the bucket water with a ratio of *r*, which means that only *r* proportion of the bucket water would finally fall into the target area. As the model integrates with time, moisture is moved horizontally and vertically between grid cells by the prevailing winds. At each time step, WAM-2layers computes the volume of the tagged water in each grid cell, in the lower and upper atmospheric buckets. The divide between lower and upper is determined by Eq. (B5) in van der Ent et al. (2014). The thickness of the layers is dynamical and determined by surface pressure. The water fluxes in each layer are the vertical integral of wind multiplied by specific humidity. Vertical exchange between the lower and upper bucket is computed from the water balance. When the source grid down below the air evaporates *e* amount of water at one time step and the ratio of the tagged water in the lower atmospheric bucket is *r*, the source grid contributes $e \times r$ of moisture that would finally fall into the target area. At the same time, the tagged water in the lower bucket would reduce the same amount of $e \times r$, and move on to the preceding time step. By the end of a model run, moisture contributions from each source grid are integrated from each time step to produce a spatial map of the overall moisture contribution to the precipitation of the target area.

2) EXPERIMENT DESIGN AND SETUP

The previous study (Zhang et al. 2017a) has compared different atmospheric data from the second version of the NCEP reanalysis (Kanamitsu et al. 2002) and ERA-I on the moisture source results over the TP, which found little difference in the moisture contributions to the region. This study focuses on comparing the effects of different surface evaporation *E* and precipitation *P* fluxes on moisture tracking. Hence, we conducted two sets of experiments with different sets of *E* and *P* fluxes. One is with observation-based data, which are the CMA precipitation and the GLDAS evaporation. The GLDAS evaporation is an output from a physically based land surface model forced by the observation variables such as precipitation, temperature, and radiation (Rodell et al. 2004; Mueller et al. 2011). To a large extent, it can be viewed as indirect observational data (Gao et al. 2014).

The other set uses the ERA-I's *E* and *P* fields. While the atmospheric data are from ERA-I, the application

of ERA-I's E and P makes the whole model input an ERA-I suite (ERA-Suite hereafter). The advantage of this suite is that the inner water cycle within ERA-I is more self-consistent, as compared to the first set of E and P data. However, the ERA-I precipitation is produced by the data-assimilation-driven general circulation model which provides unreliable precipitation values (Trenberth et al. 2011; Berrisford et al. 2011) especially over the TP (Tong et al. 2014). The consequent ERA-I evaporation faces the same problem. Thus, the experiment with ERA-Suite serves as a supplementary for comparison purpose.

When using observation data, the monthly CMA precipitation is applied to rescale the 3-h ERA-I precipitation data so as to keep the diurnal precipitation variation information. Meanwhile, the monthly precipitation amount conforms to the CMA's. The specific procedures are as follows. The CMA precipitation is first transformed to the same spatial resolution as ERA-I by taking the means of the 0.5° grids that fall into the 1° grid. Then the monthly ERA-I precipitation is calculated. By setting the monthly CMA precipitation as the norm, a divided ratio for ERA-I is produced. All the 3-h ERA-I precipitation amounts during a month are then rescaled proportionally. As the GLDAS evaporation only covers the land, evaporation fields over the ocean from ERA-I are adopted as there is no better alternative. All the input data for WAM-2layers are discretized to a 15-min time step to limit numerical errors in moisture backtracking. We used linear interpolation or equal division methods to transform the 6- or 3-h data to 15-min intervals as in previous studies (e.g., van der Ent et al. 2014; van der Ent and Tuinenburg 2017; Keys et al. 2014).

c. Methods

Linear regression is applied to measure the change magnitude of variables during the study period. Linear trends are normally given the 95% confidence intervals unless otherwise noted.

As the statistically significant grid points on a field may be spurious and the results may be overstated, the field significance test with the false discovery rate (FDR) method is applied (Wilks 2016). The FDR method is a straightforward solution by controlling the false discovery rate α_{FDR}. The procedures are as follows:

1) Compute all the grids for the p values of the local null hypotheses.
2) Sort the p values in an order of $p(1) \le p(2) \le \ldots \le p(N)$.
3) Find the threshold p value p^*_{FDR} that meets Eq. (1). If the p^*_{FDR} is found, the global null hypothesis is rejected.

The probability of rejecting a global null hypothesis if it is true is $\alpha_{\mathrm{global}} = \alpha_{\mathrm{FDR}}$ (Wilks 2006):

$$p^*_{\mathrm{FDR}} = \max_{i=1,\ldots,N}\left[p(i): p(i) \le \frac{i}{N}\alpha_{\mathrm{FDR}}\right]. \quad (1)$$

3. Results

According to the CMA precipitation, the mean annual precipitation values of NTP and STP during 1979–2016 are 228.6 and 599.9 mm, respectively. The annual precipitation series also indicates different trends with a strong upward trend of $15.1 \pm 8.2\,\mathrm{mm\,yr^{-1}\,decade^{-1}}$ significant at the 0.01 level over the NTP and a slight insignificant downward trend of $-1.0 \pm 15.8\,\mathrm{mm\,yr^{-1}\,decade^{-1}}$ over the STP (Fig. 1b). These results suggest that different climatic systems dominate the two regions and dominance may act differently in causing the different trends in precipitation.

a. Mean moisture contribution

By tracing the precipitation sources of the two targeted regions and setting proper thresholds, sources with higher moisture contribution are extracted that in all contribute around 80% of the annual precipitation (Fig. S1 in the online supplemental material; Zhang et al. 2017a,b; Keys et al. 2012, 2014). Then, for subregion division and direct comparison, the two 80% regions are combined into one basic source region as shown in Figs. 2a and 2b. Apparently, the combined region comprises two major parts. One part is to the west and north of TP, covering all of Europe, where moisture is transported to the TP by the westerlies. The other is to the south and east of TP, extending to the Indian Ocean and Indochina, where moisture is mainly transported by the Asian monsoons (the South/East Asian summer monsoons). Precipitation in the NTP is more influenced by the westerlies as the center of the mean moisture contribution is concentrated toward the northwest, while in the STP precipitation is more influenced by the Asian summer monsoons as the center moves more toward the southeast (Figs. 2a,b and Fig. S1). Moisture sources located far upwind tend to contribute less moisture to precipitations over the target regions. Thus, the target region itself or nearby areas tend to be the core area that contributes moisture the most intensively. Besides, at similar distances upwind, the water surface source contributes more than the land, as seen in the Caspian Sea and Aral Sea areas.

To further quantify the moisture contribution from regions dominated by different circulations, the basic source region is roughly divided into the northwest

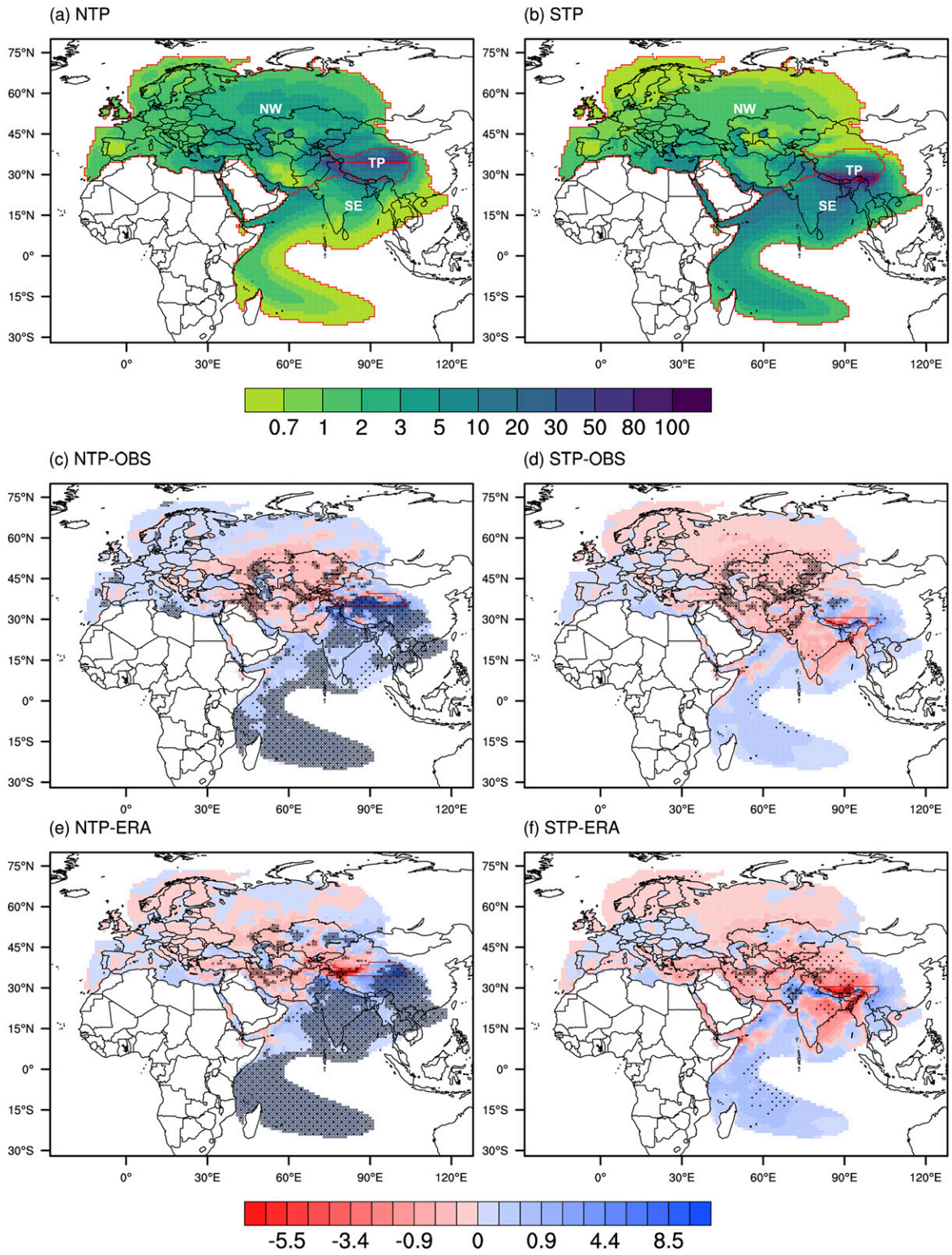

FIG. 2. Mean annual moisture contributions for (a) NTP and (b) STP using observation data from 1979 to 2016 (mm yr^{-1}). The outer red lines extract grids with higher contributions that together contribute more than 80% of the annual precipitation moisture. The inner red lines divide the extracted area into NW, SE, and the TP subregions as they represent different circulation systems. Values outside the red perimeter are not shown here or in subsequent figures. Annual moisture contribution trends for (c) NTP and (d) STP using observation data (mm yr^{-1} $decade^{-1}$). The dots indicate trends significant at the 0.05 level based on the Student's *t* test. The circles indicate trends passed the FDR test. (e),(f) As in (c) and (d), but using ERA-Suite.

(NW), the southeast (SE), and the TP as outlined in Figs. 2a and 2b. The local contributions from NTP and STP are also measured. The mean contributions during the study period from these regions are shown in Fig. 3a. For the NTP, region NW contributes 38.9% of moisture for the annual precipitation, which is the highest among the subregions. Region SE contributes 17.9% of moisture. The TP contributes about 26.1%, indicating an important role of TP in supplying moisture for the NTP. The local contribution is about 12.9%. Using ERA-Suite, contribution results are obtained as 42.6%, 16.3%, 29.6%, and 16.6% for the NW, SE, TP, and local (NTP), respectively. It differs the most in contributions from the NW and local regions with ~3.7% higher using ERA-Suite than observation data, which demonstrates the difference of using a different data source. However, the main moisture source remains unchanged.

For the STP, most moisture comes from region SE, with a contribution ratio of 51.4%. Region NW contributes only 16.9% of moisture for precipitation. The TP contributes 16.2%, indicating a smaller role of TP in supplying moisture for the STP than NTP. Moreover, the local recycling ratio is obtained as 11.9%. Analysis using ERA-Suite shows similar results with contribution ratios of 18.3%, 54.2%, 13.9%, and 9.8% for the NW, SE, TP, and local (STP), respectively.

b. *Moisture contribution trends*

The trends of moisture contribution for both NTP and STP with observation data are shown in Figs. 2c and 2d. There is a marked decrease center in central Asia for both target regions. The one for NTP is a smaller region surrounded by increasing trends, whereas the one for STP is a wider region with negative trends extending to the northern boundary. For the NTP, moisture contributions from its own regions and regions to its south and east show consistent increasing trends. However, that is not the case for STP. Moisture over India and the west Bay of Bengal shows a decreasing trend (cf. Figs. 2d and 2f), while moisture from the surrounding areas shows an increasing trend.

The comparison sets with ERA-Suite are shown in Figs. 2e and 2f. For the NTP, one point worth noting is that a strong decreasing trend is observed in the western end of NTP and its northern region (Fig. 2e), opposite to that in Fig. 2c. For the STP, the change pattern between the two datasets is mostly the same except that there is an overwhelming negative trend over the TP (Fig. 2f) in contrast with that in Fig. 2d.

To better characterize the variations in moisture contribution from the subregions, the annual moisture contribution series for both NTP and STP using the observation data is shown in Figs. 3b and 3c. The

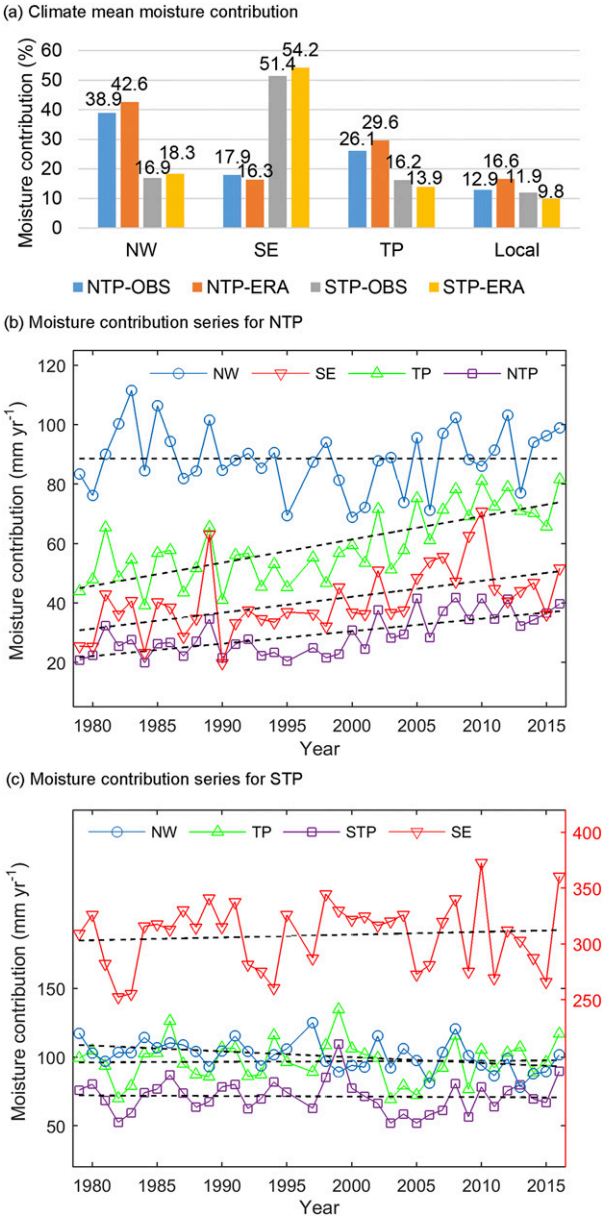

FIG. 3. (a) Mean annual moisture contributions from the subregions to both NTP and STP using both observation data and ERA-Suite. Annual moisture contribution series from the subregions for (b) NTP and (c) STP using observation data. The dashed lines are the linear fit.

contributions from the subregions are transformed into the precipitation depth over the target regions. For the NTP, region NW basically shows no trend as the moisture decrease in central Asia and the moisture increase in its surroundings counteract each other (Fig. 2c). Region SE and the TP contribute to increasing trends in moisture contribution significant at the 0.01 level with rates of 5.4 ± 2.9 and 7.8 ± 2.5 mm yr^{-1} $decade^{-1}$, respectively. They account for 35.8% and 51.7% of the

TABLE 1. Annual moisture contribution trends from the subregions to both NTP and STP (mm yr^{-1} $decade^{-1}$). Trends that are above the 0.05 significance level based on the two-tailed Student's t test are marked with * and 0.01 with **.

Contribution trend	NW	SE	TP	Local
NTP-OBS	−0.0 ± 3.2	5.4 ± 2.9**	7.8 ± 2.5**	4.2 ± 1.5**
NTP-ERA	−1.0 ± 4.9	6.6 ± 3.3**	3.1 ± 4.5	0.1 ± 2.6
STP-OBS	−4.2 ± 2.9**	2.5 ± 9.1	0.4 ± 4.6	−0.4 ± 3.6
STP-ERA	−6.0 ± 8.4	2.8 ± 27.2	−8.5 ± 7.0*	−4.3 ± 3.3**

NTP precipitation increase. Similarly, the local contribution increases significantly at the 0.01 level with a rate of 4.2 ± 1.5 mm yr^{-1} $decade^{-1}$ that accounts for 27.8% of the precipitation increase. For the STP, the only significant trend is obtained from region NW, which is at the 0.01 level with a decreasing rate of −4.2 ± 2.9 mm yr^{-1} $decade^{-1}$. Compared with its contribution to the NTP, region NW exerts different influences to the precipitation changes over the STP. Contribution from region SE shows an increasing trend of 2.5 ± 9.1 mm yr^{-1} $decade^{-1}$. Moreover, contributions from the TP and the local STP show a slight change over time in opposite signs. The statistics using both observation data and ERA-Suite are compared in Table 1. They are generally of the same signs between the two datasets, except that the TP contributes differently to the STP precipitation.

c. *Moisture contributions in the wet season*

Annual precipitation over the TP is dominated by the wet season (May–September; Zhang et al. 2017a). According to the CMA precipitation, the wet season precipitation accounts for 88.4% and 77.1% of the annual precipitation for the NTP and the STP, respectively. The respective precipitation variations during 1979–2016 are also similar. According to the linear correlation test, the correlation coefficient between the wet season and yearly precipitations is 0.98 for the NTP and 0.90 for the STP, significant at the 0.01 level. Thus, the annual precipitation can be represented by the wet-season precipitation, and moisture contribution and circulation during the wet season need further study.

Figures 4a and 4b show trends of the moisture contribution and moisture transport for the NTP and STP in the wet season during 1979–2016. In comparison with the annual trends in moisture contribution (Figs. 2c,d), the spatial patterns for either NTP or STP show strong similarity. This demonstrates that the interannual change in moisture contribution during the wet season dominates the whole year. There are southerly and easterly anomalies over the NTP, indicating more influences coming from the south and east. In central Asia, significantly strong northeasterly and easterly anomalies reduce moisture to be transported to the TP. Over the STP, southerlies and easterlies are found in the western and eastern parts, respectively. In addition, to the south of STP, strong southerly anomalies from the north Indian Ocean and Bay of Bengal tend to bring more moisture from the Indian Ocean to the TP. There are also significant easterlies east of the STP. The easterlies help bring more moisture from the east, but may have the possibility to hinder the southwest monsoon moisture transport from the Bay of Bengal (Fig. 4c).

4. Discussion

Keys et al. (2012) proposed the concept of precipitationshed, which specifies a region that encloses the upwind atmosphere and surface that contributes evaporated moisture to the target area's precipitation. Changes in land surface conditions or circulations within the precipitationshed would influence precipitation in the target area. During the last 38 years, the land surface conditions have experienced inconsistent spatial changes which end up in a spatially heterogeneous pattern of the evaporation trend (Fig. 5). Intuitively, sources within the precipitationshed with an increasing trend in evaporation should contribute more moisture to the target region, and vice versa. If the moisture transport along the path to the target region is strengthened, the moisture contribution would be amplified. Regions in central Asia show an obvious decreasing trend in evaporation, except over water surfaces such as the Black Sea and the Caspian Sea. Combined with the weakened westerly moisture transport, moisture contributed to both NTP and STP from this area decreases significantly (Figs. 4a,b). However, although moisture transport over the Caspian Sea is weakened, its moisture contribution to the NTP increases significantly (Fig. 4a). The effect of increased evaporation over the Caspian Sea during the period seems to outweigh the decreased moisture transport, which finally results in an increase in its moisture contribution. A similar situation also occurs in the Black Sea.

a. *On evaporation and precipitation data*

Trend analysis using different sets of E and P fluxes demonstrates a notable difference for the NTP's precipitation source, that is, the west end of NTP shows a

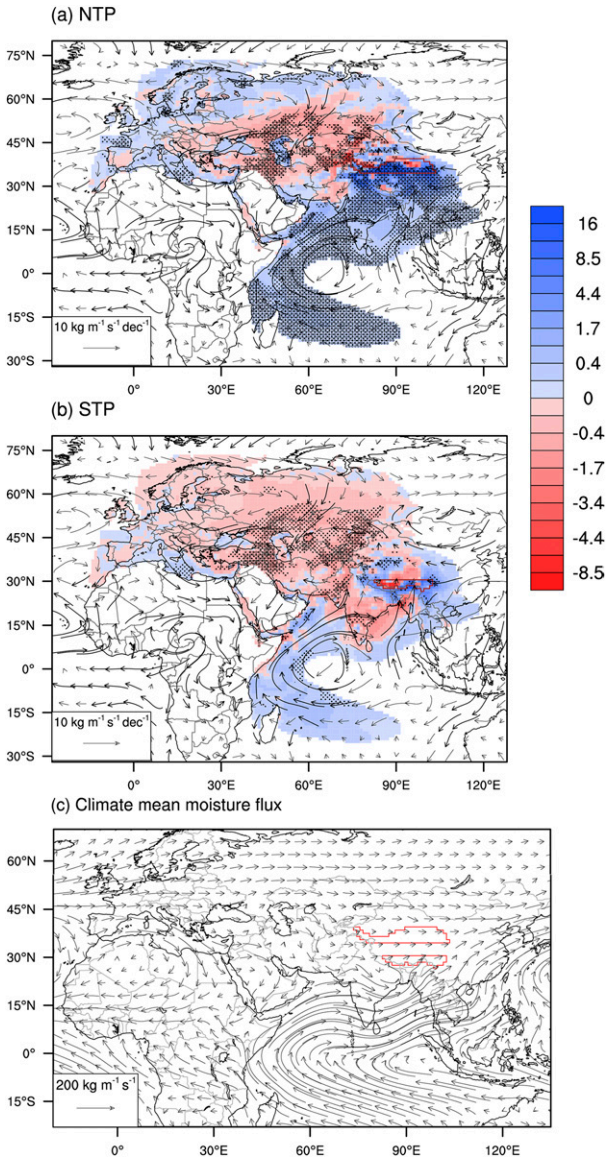

FIG. 4. Wet season moisture contribution trends during 1979–2016 for the (a) NTP and (b) STP using observation data (mm yr^{-1} $decade^{-1}$). The dots indicate trends significant at the 0.05 level based on the Student's t test. The circles indicate trends passed the FDR test. The vectors are the wet season moisture transport trends during the years. The bold vectors represent the significant anomalies at the 0.05 level based on the t test. (c) Climate mean moisture transport in the wet season.

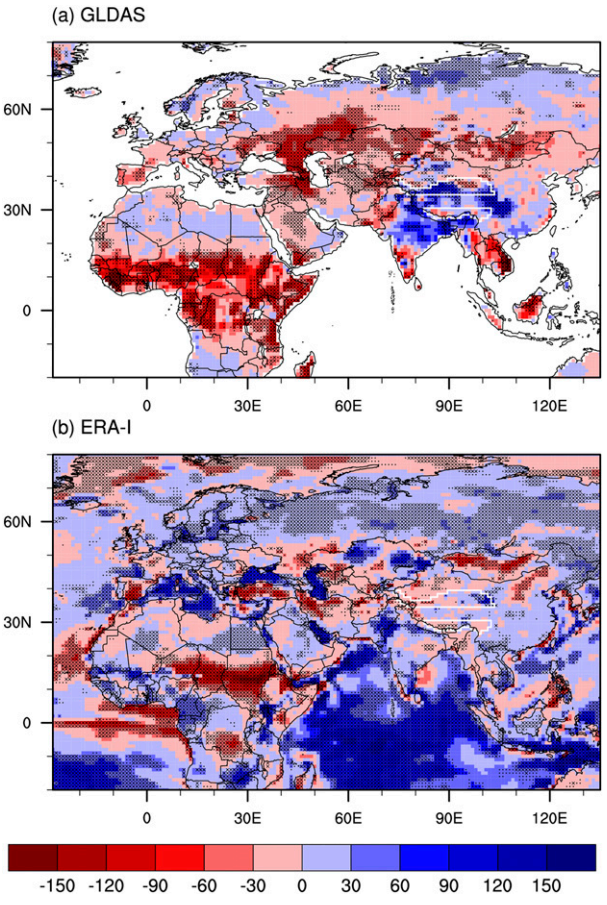

FIG. 5. Wet season evaporation trends during 1979–2016 with (a) GLDAS and (b) ERA-I data (mm yr^{-1} $decade^{-1}$). The dots indicate trends significant at the 0.05 level based on the Student's t test. The crosses indicate trends passed the FDR test.

strong positive contribution trend using observation data, but a strong negative trend using ERA-Suite (cf. Figs. 2c and 2e). In contrast, evaporation over the west NTP with GLDAS has increased strongly, while it has decreased with ERA-I (Fig. 5). The discrepancy between the evaporation trends likely caused the opposite trends of moisture contribution. Recent studies have suggested an enhanced hydrological cycle on the northwest TP with intensified precipitation and evaporation (Zhang et al. 2017a; An et al. 2017). Intensified evaporation on the northwest TP is attributed to many factors, including increased temperature, melting glacier, enlarging lakes, and enhanced evapotranspiration under the TP greening (Lei et al. 2017; Zhang et al. 2013; Zhu et al. 2016; Shen et al. 2015; An et al. 2017). The GLDAS data better capture this feature, as compared to the ERA-I, which resulted in more reliable trends in moisture contribution.

The stations over the west of NTP are extremely scarce with only one station inside the NTP, which makes the NTP precipitation doubtful for its credibility. The precipitation trend distributions from both CMA and Global Precipitation Climatology Project (GPCP) products are thus compared in Fig. 6. GPCP is a precipitation analysis based on both gauge data and satellite estimates (Huffman et al. 2009). We can

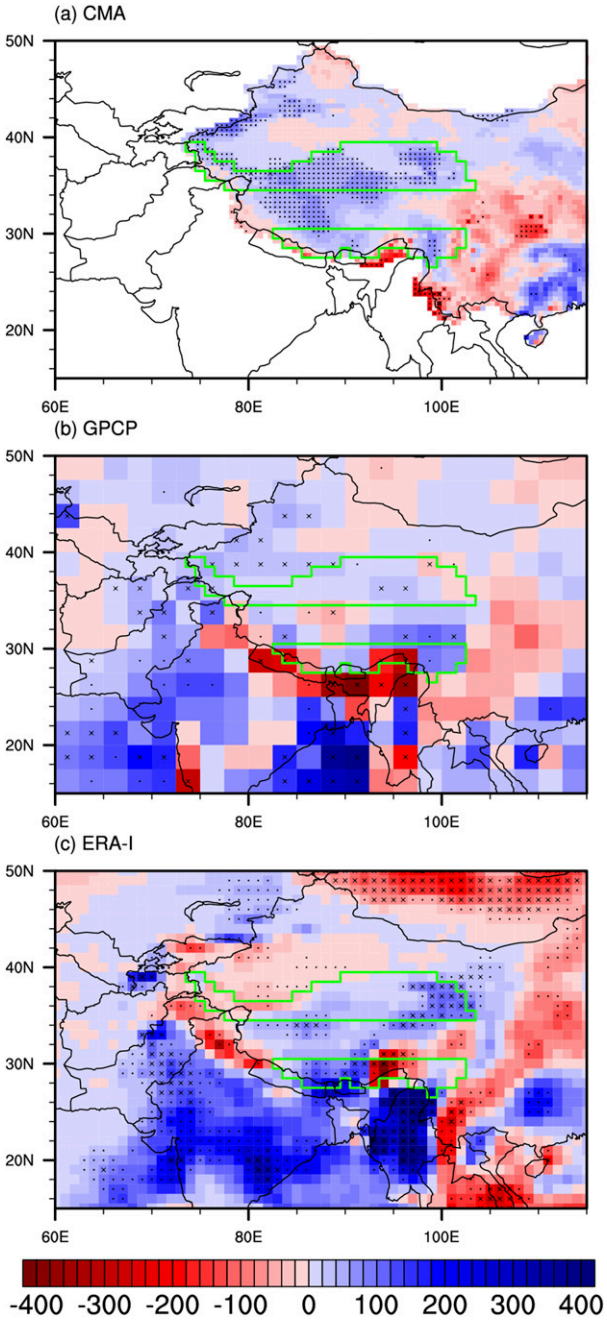

FIG. 6. Wet season precipitation trends during 1979–2016 with (a) CMA, (b) GPCP, and (c) ERA-I data (mm yr^{-1} $decade^{-1}$). The dots indicate trends significant at the 0.05 level based on the Student's t test. The crosses indicate trends passed the FDR test.

see clearly in the west NTP that the grids show an increasing trend, though the increasing magnitude may differ. The increased trend of the NTP precipitation is robust between the observational datasets. In a previous study, robustly increased precipitation was also found over the NTP among the CMA, GPCP, and

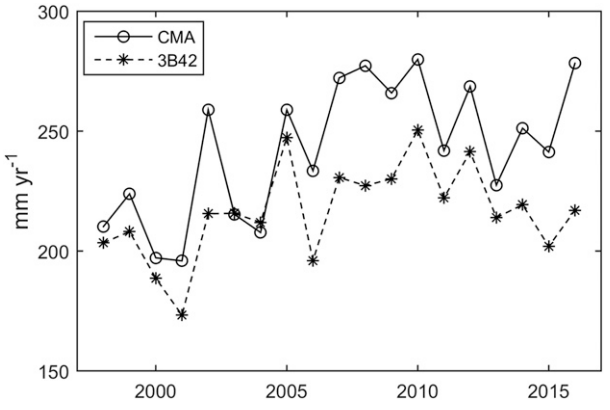

FIG. 7. The annual NTP precipitation series during 1998–2016 with the CMA and 3B42 datasets.

CMAP datasets (Fig. 7 in Zhang et al. 2017a). As we mainly focus on the precipitation change, the actual precipitation value or trend value does not count that much as long as the change is strong and the change direction is consistent.

In addition, the TRMM Multisatellite Precipitation Analysis (TMPA) 3B42 dataset (Huffman et al. 2007) at the finer grid of 0.25° × 0.25° is applied to analyze the influence of satellite-based precipitation on the NTP moisture source results. Since the 3B42 begins from 1998, the NTP precipitations during the overlapped period of 1998–2016 are compared (Fig. 7). The two series show a high similarity in the variability as the correlation coefficient between the two linearly detrended series is 0.75 significant at the 0.01 level. Though the magnitude of the linear trend of 3B42 is not as large as that of CMA, it is an increasing trend significant at the 0.1 level. This adds to the reliability of the CMA precipitation in the depiction of the NTP precipitation variation.

The climate mean of moisture contribution and the trend during 1998–2016 for the NTP are shown in Fig. 8. The climate mean moisture contribution with both datasets shows high similarities in the spatial structure. There is a small difference in the magnitude of contributed moisture in north Kazakhstan and northeast of Madagascar, which is mainly due to the difference in the precipitation amount between the two datasets (Fig. 7). The moisture contribution trend from 1998 to 2016 shows a pattern with the west of the NTP increased the most, sources west of central Asia and east of the NTP decreased, and sources to the north of Kazakhstan and in the south increased. The pattern is the same between CMA and 3B42 data, while the decreased areal extent is larger with 3B42 and the increased magnitude in the west of the NTP is stronger with CMA data. In sum, quantitative results over the

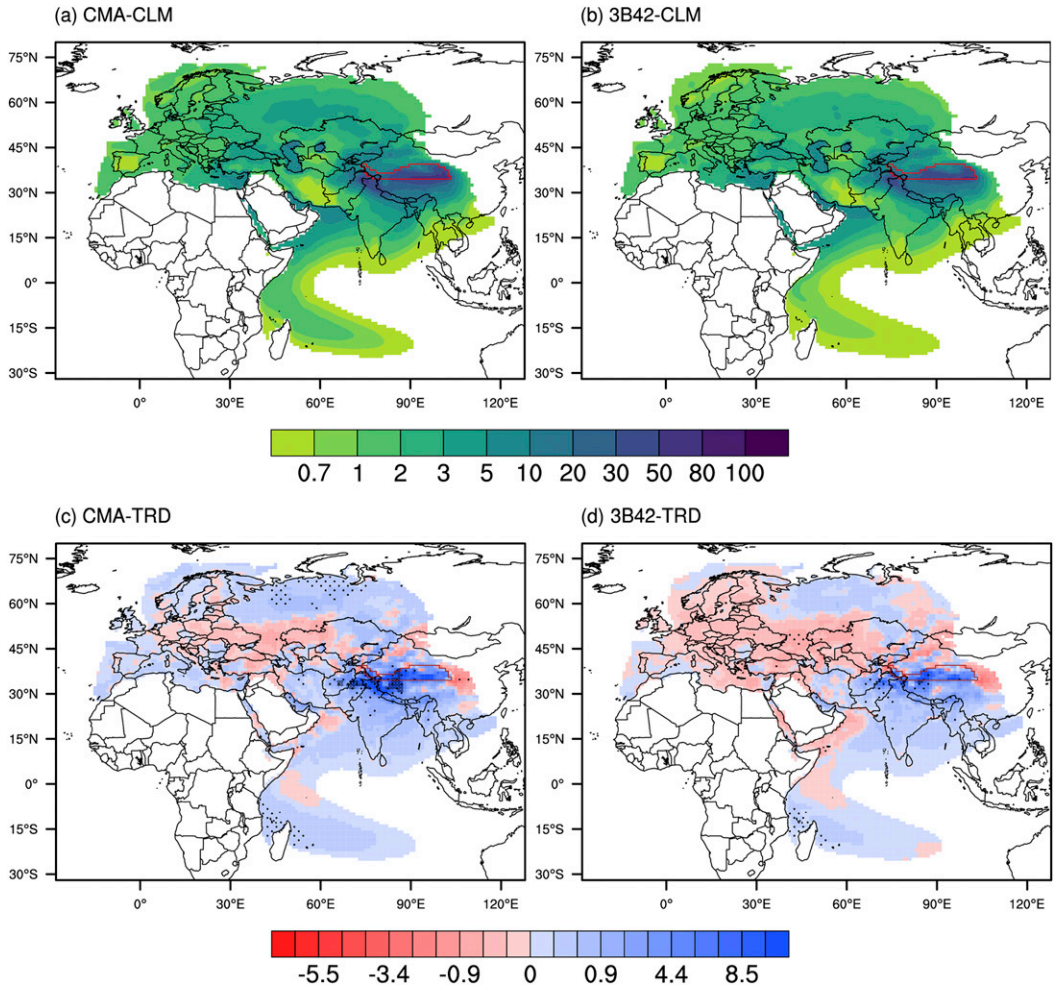

FIG. 8. Mean annual moisture contributions for the NTP with (a) CMA and (b) 3B42 precipitation data from 1998–2016 (mm yr^{-1}). Annual moisture contribution trends for the NTP with (c) CMA and (d) 3B42 precipitation data (mm yr^{-1} $decade^{-1}$). The dots indicate trends significant at the 0.05 level based on the Student's *t* test. The circles indicate trends passed the FDR test.

NTP with CMA data may be doubtful for the accuracy, but some derived qualitative findings can be reliable.

b. *Moisture contributed from India to the STP and NTP*

For the STP, both observation data and ERA-Suite show a decrease in moisture contribution from the Indian subcontinent (Figs. 2d,f), while the subcontinent contributes more moisture to the NTP (Figs. 2c,e). This is at odds with the general pattern that sources from the south and east are providing more moisture to the TP. The evaporation trends with GLDAS and ERA-I over India have shown opposite spatial patterns (Fig. 5). Moisture transport shows an overall southerly anomaly over this area, indicating more moisture is transported to the north (Fig. 4b). Neither changes in evaporation nor moisture transport can provide a satisfactory explanation for the decrease in moisture contribution from India. In fact, strengthened moisture transport does not guarantee more precipitation downwind by itself. Proper meteorological conditions are needed to facilitate the moist air to be precipitated out.

As Jiang and Ting (2017) pointed out, the summertime precipitation shows a dipole pattern between central India and the southeast TP, while there is a synchronous pattern between central India and the southwest TP. Rainfall anomalies in central India tend to induce changes in regional circulation that suppress rainfall in the southeast TP (Jiang and Ting 2017). Along the latitude of 28°N in the STP from the west to the east, the precipitation variation changes from negative to positive, from positive to negative, and from negative to positive (Fig. 6b the most typical).

Many of the trends are significant at the 0.05 level, which demonstrates the complexity of the local climates. We speculate that sources from central India may play different roles in contributing moisture for the eastern and western STP, as it may provide more moisture for one side but less for the other side. The less contributed moisture outweighs its counterpart, resulting in an overall decrease in moisture contribution from India to the STP.

For the precipitation increase over the northern TP, previous studies found it is related to the positive westerly wind anomalies over the entrance of the East Asia westerly jet (EAJ) in the upper troposphere (Wang et al. 2018). The intensified upper westerlies would motivate the secondary circulation, often causing enhanced ascending motion over the TP to bring in more precipitation (Wang et al. 2018). This process may occur with the enhanced southerly flux, originating from the Indian Ocean, to result in more precipitated moisture coming from the southern oceans. The mechanisms need further investigation in the future.

5. Conclusions

Moisture sources for precipitation over the NTP and STP and their evolutions with atmospheric moisture transport were investigated in this study. Accordingly, the following conclusions are derived:

1) Main moisture sources for precipitation over the NTP and STP are indeed different. For the NTP, region NW is the main moisture source that provides around 38.9% of moisture for the annual precipitation, followed by the whole TP (26.1%) and region SE (17.9%). The local NTP provides around 12.9% of moisture. For the STP, region SE is the primary source that provides around 51.4%, which is much higher than other subregions altogether. The NW, whole TP, and local STP provide moisture around 16.9%, 16.2%, and 11.9%, respectively.
2) The increased annual precipitation over NTP is largely attributed to the increased moisture contribution from the TP and SE regions, which contributed around 35.8% and 51.7% to the increase, respectively. At the same time, moisture contribution from region NW remained unchanged. The local contribution from NTP also increased strongly, which accounted for 27.8% of the precipitation increase. For the STP, only the moisture contribution from NW had a significant trend of $-4.2 \pm 2.9\,\mathrm{mm\,yr^{-1}\,decade^{-1}}$ at the 0.01 level. Meanwhile, the contribution from the SE has increased with a trend of $2.5 \pm 9.1\,\mathrm{mm\,yr^{-1}\,decade^{-1}}$. The TP and local region (STP) show a slight increase and decrease with trends of 0.4 ± 4.6 and $-0.4 \pm 3.6\,\mathrm{mm\,yr^{-1}\,decade^{-1}}$, respectively. The overall contribution from the subregions to the STP shows a weak downward trend of $-1.3 \pm 13.0\,\mathrm{mm\,yr^{-1}\,decade^{-1}}$.
3) Change in atmospheric moisture transport during the study period generally supports the change of moisture contribution from the external sources for both NTP and STP. A weakened westerly moisture transport in central Asia resulted in less moisture contribution from region NW for both NTP and STP, while an enhanced moisture transport from the south and east brought more moisture from region SE to the TP. However, the SE and TP regions contributed heavily and significantly to the increased precipitation in NTP, while their contributions to the STP were minor and insignificant. Moisture that originated from the Indian subcontinent changed differently for precipitations over the NTP and STP, as it provided more moisture for the NTP but less for the STP during 1979–2016.

Acknowledgments. This research is supported by the Strategic Priority Research Program of Chinese Academy of Sciences (XDA20060402), the National Natural Science Foundation of China (Grants 41701033, 4151101291, 41730645, and 41425002). Support from Swedish VR, STINT, BECC, MERGE, and SNIC through S-CMIP are also acknowledged. Ruud van der Ent acknowledges funding from the Netherlands Organization for Scientific Research (NWO), project number 016.Veni.181.015.

REFERENCES

An, W., and Coauthors, 2017: Enhanced recent local moisture recycling on the northwestern Tibetan Plateau deduced from ice core deuterium excess records. *J. Geophys. Res. Atmos.*, **122**, 12 541–12 556, https://doi.org/10.1002/2017JD027235.

Berrisford, P., P. Kållberg, S. Kobayashi, D. Dee, S. Uppala, A. J. Simmons, P. Poli, and H. Sato, 2011: Atmospheric conservation properties in ERA-Interim. *Quart. J. Roy. Meteor. Soc.*, **137**, 1381–1399, https://doi.org/10.1002/qj.864.

Bibi, S., L. Wang, X. Li, J. Zhou, D. Chen, and T. Yao, 2018: Climatic and associated cryospheric, biospheric, and hydrological changes on the Tibetan Plateau: A review. *Int. J. Climatol.*, **38**, e1–e17, https://doi.org/10.1002/joc.5411.

Boos, W. R., and Z. Kuang, 2010: Dominant control of the South Asian monsoon by orographic insulation versus plateau heating. *Nature*, **463**, 218–222, https://doi.org/10.1038/nature08707.

Bosilovich, M. G., 2002: On the vertical distribution of local and remote sources of water for precipitation. *Meteor. Atmos. Phys.*, **80**, 31–41, https://doi.org/10.1007/s007030200012.

Chen, B., X. Xu, S. Yang, and W. Zhang, 2012: On the origin and destination of atmospheric moisture and air mass over the Tibetan Plateau. *Theor. Appl. Climatol.*, **110**, 423–435, https://doi.org/10.1007/s00704-012-0641-y.

Chen, D., and Coauthors, 2015: Assessment of past, present and future environmental changes on the Tibetan Plateau.

Chin. Sci. Bull., **60**, 3025–3035, https://doi.org/10.1360/N972014-01370.

Cuo, L., Y. Zhang, Q. Wang, L. Zhang, B. Zhou, Z. Hao, and F. Su, 2013: Climate change on the northern Tibetan Plateau during 1957–2009: Spatial patterns and possible mechanisms. *J. Climate*, **26**, 85–109, https://doi.org/10.1175/JCLI-D-11-00738.1.

Dee, D. P., and Coauthors, 2011: The ERA-Interim reanalysis: Configuration and performance of the data assimilation system. *Quart. J. Roy. Meteor. Soc.*, **137**, 553–597, https://doi.org/10.1002/qj.828.

Dirmeyer, P. A., J. Wei, M. G. Bosilovich, and D. M. Mocko, 2014: Comparing evaporative sources of terrestrial precipitation and their extremes in MERRA using relative entropy. *J. Hydrometeor.*, **15**, 102–116, https://doi.org/10.1175/JHM-D-13-053.1.

Draxler, R. R., and G. D. Hess, 1998: Description of the HYSPLIT_4 modeling system of trajectories, dispersion, and deposition. *Aust. Meteor. Mag.*, **47**, 295–308.

Feng, L., and T. Zhou, 2012: Water vapor transport for summer precipitation over the Tibetan Plateau: Multidata set analysis. *J. Geophys. Res.*, **117**, D20114, https://doi.org/10.1029/2011JD017012.

Gao, Y., C. Lan, and Y. Zhang, 2014: Changes in moisture flux over the Tibetan Plateau during 1979–2011 and possible mechanisms. *J. Climate*, **27**, 1876–1893, https://doi.org/10.1175/JCLI-D-13-00321.1.

——, X. Li, L. R. Leung, D. Chen, and J. Xu, 2015: Aridity changes in the Tibetan Plateau in a warming climate. *Environ. Res. Lett.*, **10**, 034013, https://doi.org/10.1088/1748-9326/10/3/034013.

Goessling, H. F., and C. H. Reick, 2013: On the "well-mixed" assumption and numerical 2-D tracing of atmospheric moisture. *Atmos. Chem. Phys.*, **13**, 5567–5585, https://doi.org/10.5194/acp-13-5567-2013.

Held, M., and B. J. Soden, 2006: Robust responses of the hydrological cycle to global warming. *J. Climate*, **19**, 5686–5699, https://doi.org/10.1175/JCLI3990.1.

Huffman, G. J., and Coauthors, 2007: The TRMM Multisatellite Precipitation Analysis (TMPA): Quasi-global, multiyear, combined-sensor precipitation estimates at fine scales. *J. Hydrometeor.*, **8**, 38–55, https://doi.org/10.1175/JHM560.1.

——, R. F. Adler, D. T. Bolvin, and G. Gu, 2009: Improving the global precipitation record: GPCP version 2.1. *Geophys. Res. Lett.*, **36**, L17808, https://doi.org/10.1029/2009GL040000.

Jiang, X., and M. Ting, 2017: A dipole pattern of summertime rainfall across the indian subcontinent and the Tibetan Plateau. *J. Climate*, **30**, 9607–9620, https://doi.org/10.1175/JCLI-D-16-0914.1.

Kanamitsu, M., W. Ebisuzaki, J. Woollen, S.-K. Yang, J. J. Hnilo, M. Fiorino, and G. L. Potter, 2002: NCEP-DOE AMIP-II Reanalysis (R-2). *Bull. Amer. Meteor. Soc.*, **83**, 1631–1643, https://doi.org/10.1175/BAMS-83-11-1631.

Keys, P. W., R. J. van der Ent, L. J. Gordon, H. Hoff, R. Nikoli, and H. H. G. Savenije, 2012: Analyzing precipitation sheds to understand the vulnerability of rainfall dependent regions. *Biogeosciences*, **9**, 733–746, https://doi.org/10.5194/bg-9-733-2012.

——, E. A. Barnes, R. J. van der Ent, and L. J. Gordon, 2014: Variability of moisture recycling using a precipitationshed framework. *Hydrol. Earth Syst. Sci.*, **18**, 3937–3950, https://doi.org/10.5194/hess-18-3937-2014.

Klein, J. A., K. A. Hopping, E. T. Yeh, Y. Nyima, R. B. Boone, and K. A. Galvin, 2014: Unexpected climate impacts on the Tibetan Plateau: Local and scientific knowledge in findings of delayed summer. *Global Environ. Change*, **28**, 141–152, https://doi.org/10.1016/j.gloenvcha.2014.03.007.

Knoche, H. R., and H. Kunstmann, 2013: Tracking atmospheric water pathways by direct evaporation tagging: A case study for West Africa. *J. Geophys. Res. Atmos.*, **118**, 12 345–12 358, https://doi.org/10.1002/2013JD019976.

Krause, P., S. Biskop, J. Helmschrot, W.-A. Flügel, S. Kang, and T. Gao, 2010: Hydrological system analysis and modelling of the Nam Co basin in Tibet. *Adv. Geosci.*, **27**, 29–36, https://doi.org/10.5194/adgeo-27-29-2010.

Lei, Y., and Coauthors, 2017: Lake seasonality across the Tibetan Plateau and their varying relationship with regional mass changes and local hydrology. *Geophys. Res. Lett.*, **44**, 892–900, https://doi.org/10.1002/2016GL072062.

Liu, X., and Z. Y. Yin, 2001: Spatial and temporal variation of summer precipitation over the eastern Tibetan Plateau and the North Atlantic Oscillation. *J. Climate*, **14**, 2896–2909, https://doi.org/10.1175/1520-0442(2001)014<2896:SATVOS>2.0.CO;2.

Lorenz, C., and H. Kunstmann, 2012: The hydrological cycle in three state-of-the-art reanalyses: Intercomparison and performance analysis. *J. Hydrometeor.*, **13**, 1397–1420, https://doi.org/10.1175/JHM-D-11-088.1.

Mueller, B., and Coauthors, 2011: Evaluation of global observations-based evapotranspiration datasets and IPCC AR4 simulations. *Geophys. Res. Lett.*, **38**, L06402, https://doi.org/10.1029/2010GL046230.

Rienecker, M. M., and Coauthors, 2011: MERRA: NASA's Modern-Era Retrospective Analysis for Research and Applications. *J. Climate*, **24**, 3624–3648, https://doi.org/10.1175/JCLI-D-11-00015.1.

Rodell, M., and Coauthors, 2004: The Global Land Data Assimilation System. *Bull. Amer. Meteor. Soc.*, **85**, 381–394, https://doi.org/10.1175/BAMS-85-3-381.

Seager, R., and G. A. Vecchi, 2010: Greenhouse warming and the 21st century hydroclimate of southwestern North America. *Proc. Natl. Acad. Sci. USA*, **107**, 21 277–21 282, https://doi.org/10.1073/pnas.0910856107.

Shen, M., and Coauthors, 2015: Evaporative cooling over the Tibetan Plateau induced by vegetation growth. *Proc. Natl. Acad. Sci. USA*, **112**, 9299–9304, https://doi.org/10.1073/pnas.1504418112.

Sodemann, H., C. Schwierz, and H. Wernli, 2008: Interannual variability of Greenland winter precipitation sources: Lagrangian moisture diagnostic and North Atlantic Oscillation influence. *J. Geophys. Res.*, **113**, D03107, https://doi.org/10.1029/2007JD008503.

Stohl, A., and P. James, 2004: A Lagrangian analysis of the atmospheric branch of the global water cycle. Part I: Method description, validation, and demonstration for the August 2002 flooding in central Europe. *J. Hydrometeor.*, **5**, 656–678, https://doi.org/10.1175/1525-7541(2004)005<0656:ALAOTA>2.0.CO;2.

——, and ——, 2005: A Lagrangian analysis of the atmospheric branch of the global water cycle. Part II: Moisture transports between Earth's ocean basins and river catchments. *J. Hydrometeor.*, **6**, 961–984, https://doi.org/10.1175/JHM470.1.

Sun, B., and H. Wang, 2014: Moisture sources of semiarid grassland in China using the Lagrangian particle model FLEXPART. *J. Climate*, **27**, 2457–2474, https://doi.org/10.1175/JCLI-D-13-00517.1.

Sun, Y., and Y. H. Ding, 2011: Responses of South and East Asian summer monsoons to different land–sea temperature increases under a warming scenario. *Chin. Sci. Bull.*, **56**, 2718–2726, https://doi.org/10.1007/s11434-011-4602-0.

Tong, K., F. Su, D. Yang, L. Zhang, and Z. Hao, 2014: Tibetan Plateau precipitation as depicted by gauge observations, reanalyses and satellite retrievals. *Int. J. Climatol.*, **34**, 265–285, https://doi.org/10.1002/joc.3682.

Trenberth, K. E., J. T. Fasullo, and J. Mackaro, 2011: Atmospheric moisture transports from ocean to land and global energy flows in reanalyses. *J. Climate*, **24**, 4907–4924, https://doi.org/10.1175/2011JCLI4171.1.

van der Ent, R. J., and O. A. Tuinenburg, 2017: The residence time of water in the atmosphere revisited. *Hydrol. Earth Syst. Sci.*, **21**, 779–790, https://doi.org/10.5194/hess-21-779-2017.

——, H. H. G. Savenije, B. Schaefli, and S. C. Steele-Dunne, 2010: Origin and fate of atmospheric moisture over continents. *Water Resour. Res.*, **46**, W09525, https://doi.org/10.1029/2010WR009127.

——, O. A. Tuinenburg, H. R. Knoche, H. Kunstmann, and H. H. G. Savenije, 2013: Should we use a simple or complex model for moisture recycling and atmospheric moisture tracking? *Hydrol. Earth Syst. Sci.*, **17**, 4869–4884, https://doi.org/10.5194/hess-17-4869-2013.

——, L. Wang-Erlandsson, P. W. Keys, and H. H. G. Savenije, 2014: Contrasting roles of interception and transpiration in the hydrological cycle – Part 2: Moisture recycling. *Earth Syst. Dyn.*, **5**, 281–326, https://doi.org/10.5194/esdd-5-281-2014.

Wang, A., and X. Zeng, 2012: Evaluation of multi-reanalysis products with in situ observations over the Tibetan Plateau. *J. Geophys. Res.*, **117**, D05102, https://doi.org/10.1029/2011JD016553.

Wang, T., J. P. Miao, J. Q. Sun, and Y. H. Fu, 2018: Intensified East Asian summer monsoon and associated precipitation mode shift under the 1.5 °C global warming target. *Adv. Climate Change Res.*, **9**, 102–111, https://doi.org/10.1016/j.accre.2017.12.002.

Wei, J., P. A. Dirmeyer, M. G. Bosilovich, and R. Wu, 2012: Water vapor sources for Yangtze River Valley rainfall: Climatology, variability, and implications for rainfall forecasting. *J. Geophys. Res.*, **117**, D05126, https://doi.org/10.1029/2011JD016902.

Wilks, D. S., 2006: On ''field significance'' and the false discovery rate. *J. Appl. Meteor. Climatol.*, **45**, 1181–1189, https://doi.org/10.1175/JAM2404.1.

——, 2016: ''The stippling shows statistically significant grid points'': How research results are routinely overstated and overinterpreted, and what to do about it. *Bull. Amer. Meteor. Soc.*, **97**, 2263–2273, https://doi.org/10.1175/BAMS-D-15-00267.1.

Xu, X., T. Zhao, C. Lu, Y. Guo, B. Chen, R. Liu, Y. Li, and X. Shi, 2014: An important mechanism sustaining the atmospheric ''water tower'' over the Tibetan Plateau. *Atmos. Chem. Phys.*, **14**, 11 287–11 295, https://doi.org/10.5194/acp-14-11287-2014.

Yang, K., B. Ye, D. Zhou, B. Wu, T. Foken, J. Qin, and Z. Zhou, 2011: Response of hydrological cycle to recent climate changes in the Tibetan Plateau. *Climatic Change*, **109**, 517–534, https://doi.org/10.1007/s10584-011-0099-4.

Yao, T. D., and Coauthors, 2012: Different glacier status with atmospheric circulations in Tibetan Plateau and surroundings. *Nat. Climate Change*, **2**, 663–667, https://doi.org/10.1038/nclimate1580.

——, and Coauthors, 2013: A review of climatic controls on $\delta^{18}O$ in precipitation over the Tibetan Plateau: Observations and simulations. *Rev. Geophys.*, **51**, 525–548, https://doi.org/10.1002/rog.20023.

Yin, Y., S. Wu, D. Zhao, D. Zheng, and T. Pan, 2012: Impact of climate change on actual evapotranspiration on the Tibetan Plateau during 1981–2010 (in Chinese). *Acta Geogr. Sin.*, **67** (11), 1471–1481.

Zhang, C., Q. Tang, and D. Chen, 2017a: Recent changes in the moisture source of precipitation over the Tibetan Plateau. *J. Climate*, **30**, 1807–1819, https://doi.org/10.1175/JCLI-D-15-0842.1.

——, ——, ——, L. Li, X. Liu, and H. Cui, 2017b: Tracing changes in atmospheric moisture supply to the drying southwest China. *Atmos. Chem. Phys.*, **17**, 10 383–10 393, https://doi.org/10.5194/acp-17-10383-2017.

Zhang, G., Y. Zhang, J. Dong, and X. Xiao, 2013: Green-up dates in the Tibetan Plateau have continuously advanced from 1982 to 2011. *Proc. Natl. Acad. Sci. USA*, **110**, 4309–4314, https://doi.org/10.1073/pnas.1210423110.

Zhao, Y., and J. Zhu, 2015: Assessing quality of grid daily precipitation datasets in China in recent 50 years (in Chinese). *Plateau Meteor.*, **24**, 837–845.

——, ——, and Y. Xu, 2014: Establishment and assessment of the grid precipitation datasets in China for recent 50 years (in Chinese). *J. Meteor. Sci.*, **34**, 414–420.

Zhou, X., Y. Zhang, Y. Yang, Y. Yang, and S. Han, 2013: Evaluation of anomalies in GLDAS-1996 dataset. *Water Sci. Technol.*, **67**, 1718–1727, https://doi.org/10.2166/wst.2013.043.

Zhu, Z., and Coauthors, 2016: Greening of the Earth and its drivers. *Nat. Climate Change*, **6**, 791–795, https://doi.org/10.1038/nclimate3004.